Chapter 2 Synthesis and Characterization Techniques

Two-dimensional transition metal dichalcogenides (TMDs) nanomaterials have unveiled exceptional traits, sparking a revolution in energy generation and energy storage. This chapter deals with the description of the methods used for the synthesis and characterization of pristine $MoSe_2$, *In-situ* grown $MoSe_2$ over different conducting substrates, bimetal oxides ($CoFe_2O_4$ and $NiFe_2O_4$, $NiCo_2O_4$/NiO), hybrid nanostructures ($CoFe_2O_4$-$MoSe_2$ and $NiFe_2O_4$-$MoSe_2$, $NiCo_2O_4$/NiO-$MoSe_2$) and Ni-$MoSe_2$ nanocomposites for hydrogen evolution reaction (HER), oxygen evolution reaction (OER), electrolyzer and Zinc-air battery applications. In the present work, we have synthesized these nanomaterials via hydrothermal technique and details of the synthesis procedure has been discussed in this chapter. Fundamentals related to different characterization techniques like scanning electron microscopy (SEM), transmission electron microscopy (TEM), X-ray diffraction (XRD), Raman and Fourier transform infrared (FTIR) spectroscopy along with different electrochemical methods like linear sweep voltammetry (LSV), cyclic voltammetry (CV), electrochemical impedance spectroscopy (EIS) and galvanostatic charge/discharge techniques have been discussed in this chapter.

2.1 Materials synthesis

Material synthesis is a critical aspect of materials science and engineering, focusing on creating materials with specific properties and structures. The key to successful material synthesis is selecting the right approach and carefully controlling the synthesis conditions to achieve the desired outcome. There are two different methods: top-down and bottom-up approaches for the synthesis of nanomaterials.

Top-Down Approach

This method starts with a bulk material and reduces it to the nanoscale. Techniques include milling, etching, and lithography. While this approach is straightforward and can produce large quantities of nanomaterials, it often results in a lack of control over the final product's size, shape, and crystallinity of $MoSe_2$.

Bottom-Up Approach

This method involves assembling atoms or molecules into nanostructured materials. Techniques include atomic layer deposition, chemical vapor deposition, sol-gel synthesis, solution chemical (hydrothermal/solvothermal). This approach allows for precise control over the material's properties but can be complex and time-consuming.

In the present work, we have synthesized all nanomaterials by hydrothermal method using respective precursor and reducing agents.

2.1.1 Hydrothermal synthesis of nanostructures

It is essentially a solution reaction-based approach, where the formation of nanomaterials can occur over a wide range of temperature, from ambient temperature to very high temperatures. The process involves the use of a sealed vessel (stainless steel), known as an autoclave, where the reaction mixture is heated to high temperatures and pressures. **Figure 2.1** illustrates the hydrothermal cell that is utilized for the synthesis of $MoSe_2$ and bimetal oxides. This environment facilitates the dissolution and recrystallization of materials, leading to the formation of nanostructures. One of the significant advantages of hydrothermal synthesis is its ability to generate nanomaterials which are not stable at very high temperature. This method can produce nanomaterials with minimal loss of materials at high vapor pressures. The compositions of the synthesized nanomaterials can be well controlled through liquid phase or multiphase chemical reactions.

Figure 2.1 *Photograph of the used hydrothermal cell*

2.1.1.1 Precursor required for preparation of desired materials

Sodium molybdate dihydrate ($Na_2MoO_4 \cdot 2H_2O$), Selenium powder, Hydrazine hydrate ($N_2H_4 \cdot H_2O$), Methanol (CH_3OH), deionized (DI), Cobalt chloride ($CoCl_2.6H_2O$), Iron chloride ($FeCl_3$), Potassium hydroxide (KOH) and urea (NH_2CONH_2)

2.1.1.2 Synthesis of pristine $MoSe_2$ nanosheets

In the present work, we have synthesized $MoSe_2$ nanosheets by modifying the hydrothermal process reported in the literature, as shown in **Figure 2.2** [73, 74]. In this modified process, 0.02 M of sodium molybdate dihydrate ($Na_2MoO_4.2H_2O$) and 0.04 M of selenium powders are dissolved into a mixture of 60 mL methanol (CH_3OH), 40 mL deionized (DI) water, and 20 mL of hydrazine hydrate ($N_2H_4 \cdot H_2O$). The complete solution is stirred at 60 °C for 30 minutes and thereafter transferred in a 200 mL Teflon-lined stainless-steel autoclave to treat at 220 °C for 48 h to obtain desired $MoSe_2$ nanosheets. The autoclave was allowed to cool to ambient temperature naturally. The sample is washed with DI water and ethanol repeatedly to achieve pH neutrality and then dried at 50 °C for 12 h in a vacuum oven. The reactions involved in the hydrothermal synthesis of $MoSe_2$ are given below [75].

$$5N_2H_4 + 2Se \rightarrow N_2 \uparrow + 4N_2H_5^+ + 2Se^{2-} \quad (2.1)$$

$$2MoO_4^{2-} + N_2H_4 + 4H_2O \rightarrow 2Mo^{4+} + N_2 \uparrow + 12OH^- \quad (2.2)$$

$$Mo^{4+} + 2Se^{2-} \rightarrow MoSe_2 \quad (2.3)$$

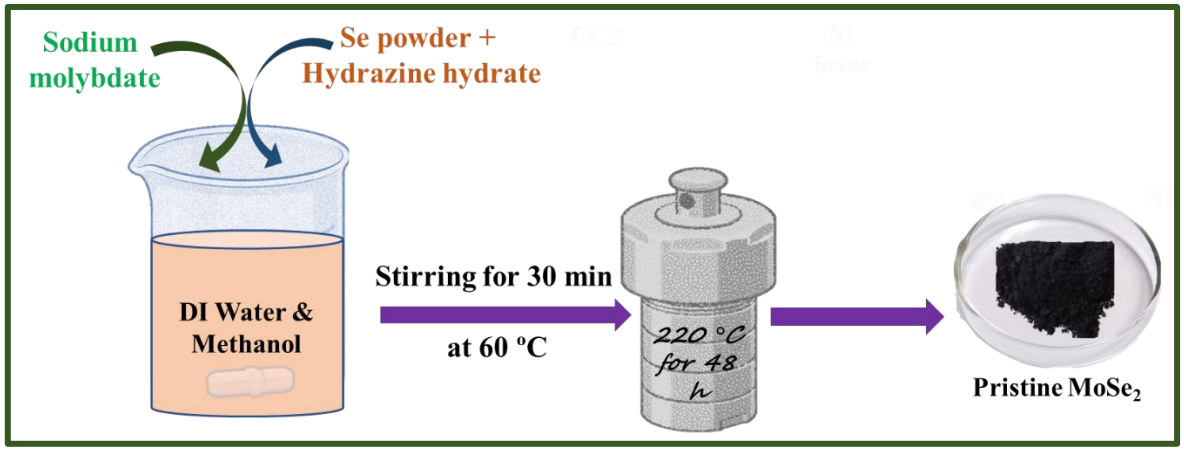

Figure. 2.2 *Schematic diagram for hydrothermal synthesis of pristine $MoSe_2$ nanosheets.*

2.1.1.3 Synthesis of *in-situ* grown vertical $MoSe_2$ over different substrates

Hydrothermal process has been used for growing vertical $MoSe_2$ on CCP and Ni foam substrates, as shown schematically in **Figure 2.3**. Conducting carbon paper and Ni foam are pre-treated in the ultrasonic bath with acetone, sulphuric acid, and methanol subsequently for 15 min each to remove surface impurities. We have grown $MoSe_2$ on pre-treated substrate by modifying the hydrothermal process reported in the previous literatures [73-77]. Initially, 40 mM solution of Selenium (Se) powder is prepared in hydrazine hydrate. Next, the resulting solution is added dropwise in 20 mM solution of $Na_2MoO_4.2H_2O$ in 80 ml of deionized (DI) water/methanol mixture (3:2 ratio of DI water: methanol). Pre-treated substrates serving as template and above solution are kept in Teflon lined autoclave and heated to 220 °C for 48 hours. The prepared binder free electrodes are separated from remaining solution and washed several times with water and methanol to eliminate impurities and make them pH neutral followed by drying at 60 °C for 10 hours in vacuum oven.

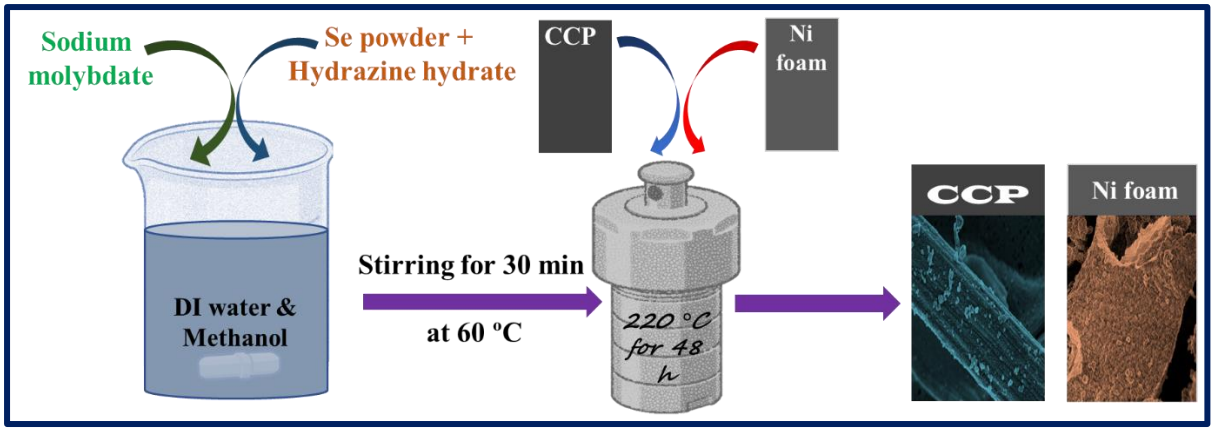

Figure 2.3 *Schematic diagram for in-situ synthesis of $MoSe_2$ on CCP and Ni foam substrates.*

2.1.1.4 Synthesis of $CoFe_2O_4$

The previously reported procedure has been followed for synthesizing $CoFe_2O_4$ using hydrothermal process.3 In this process, 0.1M Cobalt chloride ($CoCl_2.6H_2O$, Loba Chemie), 0.2 M Iron chloride ($FeCl_3$, Loba Chemie), and 1M potassium hydroxide (KOH, Loba Chemie) are dissolved and stirred in deionized water (50 mL). The obtained solution is treated at 150 °C for 12 h in a Teflon-lined stainless-steel autoclave. After repeated washing with deionized water and methanol, the $CoFe_2O_4$ black powder is vacuum-dried at 60 °C for 6 h.

2.1.1.5 Synthesis of $NiCo_2O_4$/NiO

In this process, 0.1M Cobalt chloride ($CoCl_2.6H_2O$, Loba Chemie), 0.05M Nickle chloride ($NiCl_2 \cdot 6H_2O$, Loba Chemie), and 0.18M urea (NH_2CONH_2, Loba Chemie) are stirred and dissolved in deionized water (50 mL). The obtained solution is treated at 150 °C for 12 h in a Teflon-lined stainless-steel autoclave. After repeated washing with deionized water and methanol, the sample is vacuum dried at 60 °C for 6 h. Subsequently, the dried sample was air calcined in a tubular furnace at 650 °C for 5 h to obtain $NiCo_2O_4$/NiO black powder.

2.1.1.6 Synthesis of $NiFe_2O_4$

The previously reported procedure has been followed for synthesizing $NiFe_2O_4$ using hydrothermal process.3 In this process, 0.1M Cobalt chloride ($NiCl_2.6H_2O$, Loba Chemie), 0.2

M Iron chloride ($FeCl_3$, Loba Chemie), and 1M potassium hydroxide (KOH, Loba Chemie) dissolved and stirred in deionized water (50 mL). The obtained solution is treated at 150 °C for 12 h in a Teflon-lined stainless-steel autoclave. After repeated washing with deionized water and methanol, the $NiFe_2O_4$ black powder is vacuum-dried at 60 °C for 6 h.

2.1.1.7 Synthesis of $CoFe_2O_4$-$MoSe_2$ hybrid nanostructure

To observe the synergistic effect between pristine $MoSe_2$ and $CoFe_2O_4$, we have synthesized $MoSe_2$-$CoFe_2O_4$ hybrid nanostructure (1:1 ratio). A straightforward, inexpensive, scalable physical mixing process is used to prepare hybrid nanostructure. In this method, hydrothermally prepared $CoFe_2O_4$ and $MoSe_2$ powders are weighed equally (1:1 ratio) and mixed by grinding, followed by 15 min intensive probe sonication in IPA solution for the preparation of $CoFe_2O_4$-$MoSe_2$ hybrid nanostructure. The resulting $CoFe_2O_4$-$MoSe_2$ hybrid nanostructure is separated from solution by centrifugation at 3000 rpm for 5 min, followed by vacuum drying at 60 °C for 6 h.

2.1.1.8 Synthesis of $NiCo_2O_4$/NiO-$MoSe_2$ hybrid nanostructure

In order to get homogeneous $NiCo_2O_4$/NiO-$MoSe_2$ hybrid nanostructure, 1:1 wt. ratio $MoSe_2$ and $NiCo_2O_4$/NiO of have been prepared. In this method, hydrothermally prepared $NiCo_2O_4$/NiO and $MoSe_2$ powders are weighed equally (1:1 ratio) and mixed by grinding followed by sonication for 30 minutes in ultrasonic bath in IPA solution for the preparation of $NiCo_2O_4$/NiO-$MoSe_2$ hybrid nanostructure. The resulting $NiCo_2O_4$/NiO-$MoSe_2$ hybrid nanostructure is separated from solution by centrifugation at 3000 rpm for 5 min, followed by vacuum drying at 60 °C for 6 h.

2.1.1.9 Synthesis of $NiFe_2O_4$-$MoSe_2$ hybrid nanostructure

To observe the synergistic effect between pristine $MoSe_2$ and $CoFe_2O_4$, we have synthesized $MoSe_2$-$CoFe_2O_4$ hybrid nanostructure (1:1 ratio). In this method, hydrothermally prepared $NiFe_2O_4$ and $MoSe_2$ powders are weighed equally (1:1 ratio) and mixed by grinding

followed by 15 min intensive probe sonication in IPA solution for the preparation of $NiFe_2O_4$-$MoSe_2$ hybrid nanostructure. The resulting $NiFe_2O_4$-$MoSe_2$ hybrid nanostructure is separated by centrifugation at 3000 rpm for 5 min, followed by vacuum drying at 60 °C for 6 h.

2.1.1.10 Synthesis of Ni decoration $MoSe_2$ nanocomposites

To observe the synergistic effect between pristine $MoSe_2$ and Ni nanoparticles, we have synthesized Ni-$MoSe_2$ nanocomposites (5%, 10% and 20%). To prepare Ni-$MoSe_2$ (5%) nanocomposite, 190 mg of hydrothermally prepared $MoSe_2$ powder and 41.2 mg of $NiCl_2.6H_2O$ are dissolved and stirred in deionized water (50 mL). 1M Sodium borohydride ($NaBH_4$) solution of 50 ml has been added dropwise, while stirring. The obtained solution is kept at 150 °C for 12 h in a Teflon-lined stainless-steel autoclave. After repeated washing with deionized water and methanol, the black powder is vacuum-dried at 60 °C for 6 h. Similarly, Ni-$MoSe_2$ (10%) and Ni-$MoSe_2$ (20%) nanocomposites have been prepared.

2.2 Characterization techniques

The synthesized pristine $MoSe_2$, *in-situ* grown $MoSe_2$ over conducting substrates (CCP, Ni foam), bimetal oxides, bimetal oxide-$MoSe_2$ hybrid nanostructures and Ni-$MoSe_2$ nanocomposites have been examined using various microscopy, spectroscopy, and electrochemical tools to validate their structural, morphological, and electrochemical attributes. The different characterization techniques employed in this study are briefly outlined below.

2.2.1 X-ray diffraction (XRD)

X-ray Diffraction (XRD) is a well-accepted, non-destructive, and non-contact method for characterizing materials. It is primarily employed to identify various phases, grain size, phase composition, and defect structure within a material. The obtained graph from an XRD analysis, known as a diffractogram, displays intensity as a function of angle (2θ). The XRD system comprises three main components: the X-ray generator tube, the sample stage, and the X-ray

detector. The process begins with X-rays being generated within a cathode ray tube (CRT) by the collision of high-energy electrons (generated by a high-voltage field) with a metal target. The rapid deceleration of electrons on the target converts the kinetic energy of the electrons into X-ray radiation. These X-rays are then directed towards the crystal. When the X-rays encounter the crystal, they are diffracted by the crystal lattice, the repeating pattern of atoms within the crystal. The angles at which the X-rays are diffracted depend on the size and structure of the lattice. The diffracted X-rays are then detected and recorded (counts per second), often by a rotating detector in Bragg-Brentano geometry that measures the intensity of the X-rays at different angles. This produces a diffraction pattern consisting of series of peaks at different angles (2θ). A schematic diagram of the XRD measurement is depicted in **Figure 2.4(a)**.

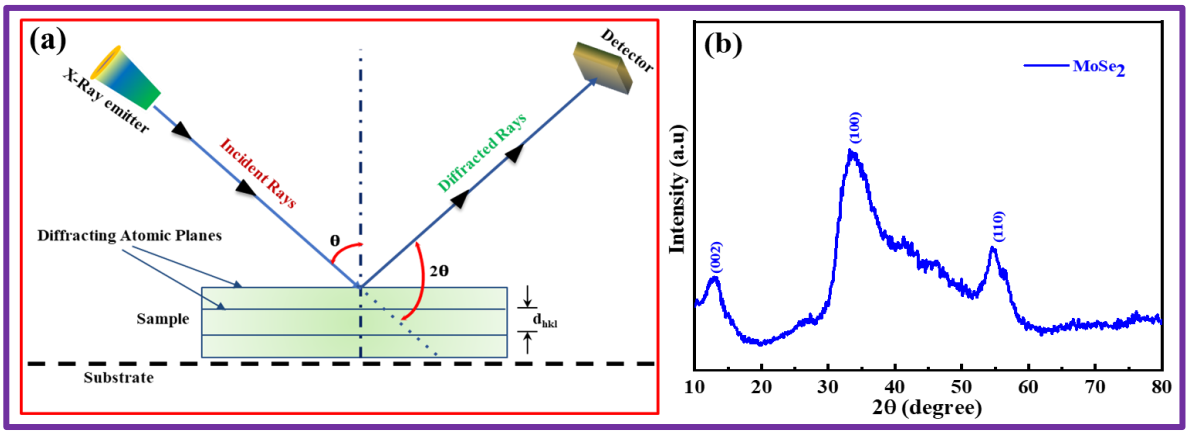

Figure 2.4 *(a)Schematic representation of X-ray diffraction process and (b) XRD pattern for pristine* $MoSe_2$.

Bragg's law (**equation 2.4**) provides the condition for diffraction of X-rays with crystal lattice, as follows:

$$n\lambda = 2d \sin\theta \tag{2.4}$$

Where, n is the order of diffraction, d is the interplanar spacing, λ is the X-rays wavelength, and θ is the angle of incidence of the X-ray beam and 2θ is the diffraction angle. Consequently, a characteristic pattern is generated, which is unique to the crystal structure present in the

sample. This pattern aids in identification when compared to a reference crystalline form. In the present work, the crystalline structures of prepared materials are examined at a scanning rate of 3° min^{-1} using a Rigaku MiniFlex-600 diffractometer with Cu-Kα radiation in the 2θ range of 10-80° with the step size of 0.02°. As an example, the XRD pattern (**Figure 2.4 (b)**) of pristine $MoSe_2$ shows the characteristic peaks at 12.8°, 33.6°, and 55.2°, corresponding to different (h k l) planes of $MoSe_2$, indicating the formation of the 2H phase of $MoSe_2$. The details of XRD analysis of other prepared materials have been discussed in respective chapters.

2.2.2 Scanning electron microscopy (SEM)

Scanning Electron Microscopy (SEM) is a tool utilized to understand the morphological characteristics of samples. It generates images of a material by scanning it with a highly focused beam of electrons emitted from an electron gun consisting of a tungsten filament cathode, as shown in **Figure 2.5 (a)**. These electrons are accelerated towards the materials using a positive electrical field. Secondary electrons are generated through inelastic scattering and possess an energy level of a few KeV, with an interaction zone ranging from 5 to 50 nm. On the other hand, backscattered electrons are produced via elastic scattering. Their high energy allows them to deviate from approximately 50 to 300 nm depths. The electron beam in the SEM carries both energy and momentum. It strikes the sample and imparts energy and momentum to the sample atoms. Furthermore, auger electrons are also generated in molecules with a low atomic number. The quality of an image in SEM is determined by the depth of field and resolution, which can be adjusted by manipulating operational variables such as the size of the final aperture, working distance, accelerating voltage, probe current, and astigmatism. However, SEM also has its limitations. The most significant limitation is that SEM requires samples to be electrically conducting, at least on the surface, and electrically grounded to prevent electrostatic charge accumulation at the material's surface. When materials/specimens lack conductivity, they are initially coated with an extremely thin layer of conducting material, such

as gold or silver. This conducting coating is applied to the specimen through one of two methods: low-vacuum sputter coating or high-vacuum evaporation. The conducting coating creates a pathway for the electron beam to travel, preventing the build-up of static charge. In the present work, prepared materials are studied using a Nova NanoSEM 450 to study the surface morphology of newly synthesized materials. As an example, SEM image of pristine $MoSe_2$ suggest the formation of interconnected wrinkled few layers nanosheets morphology, as shown in **Figure 2.5 (b)**. The SEM analysis of all prepared materials has been discussed in upcoming chapters.

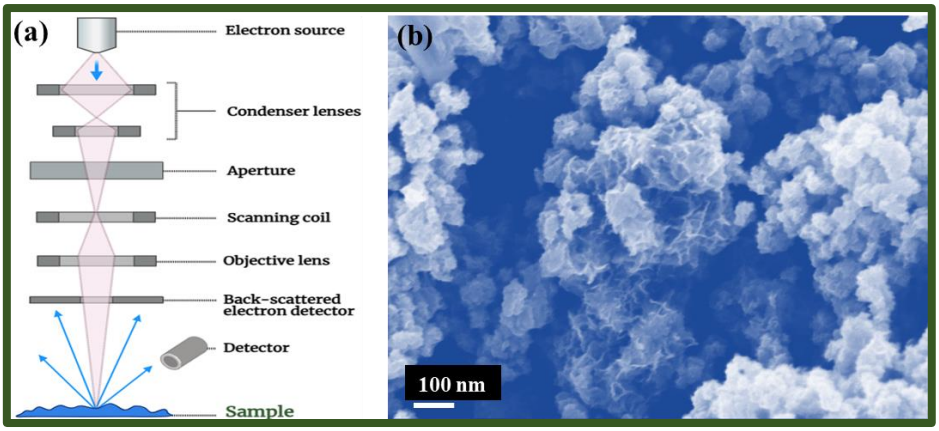

Figure 2.5 (a) *Schematic diagram of SEM and (b) SEM image of pristine* $MoSe_2$.

2.2.3 Transmission electron microscopy (TEM)

Transmission Electron Microscopy (TEM) is a powerful and widely acceptable imaging technique used in the field of nanomaterials. It operates on the principle of using a beam of electrons, to visualize specimens and generate highly magnified images, as shown in **Figure 2.6 (a)**. The TEM technique was first developed by Max Knoll and Ernst Ruska in Germany in 1931. It revolutionized the world of microscopy by providing an unprecedented resolution (up to atomic level) with magnification ~10 to 50 million times, far exceeding that of light microscopes. In a TEM, a high-voltage electron beam is emitted by a cathode and focused by electromagnetic lenses. The beam passes through the ultra-thin specimen and interacts with the specimen. This beam is then magnified and focused onto an imaging device, such as a

fluorescent screen. One of the key components of a TEM is the electron source. Modern TEMs typically use field emission guns, which provide a coherent and high-intensity electron beam. The electrons are accelerated towards the specimen by an anode, typically at voltages of 100-300 kV. The specimen must be very thin, usually less than 100 nm, and to be electron transparent. The electron beam interacts with the specimen/materials, which generates various signals. These include diffracted electrons, transmitted electrons, and secondary electrons. Each of these signals provides different information about the specimen. For example, the transmitted electrons can be used to form a phase contrast image, while the diffracted electrons can give information about the crystallography of the specimen. However, TEM also has its limitations. The main one is the need for extremely thin specimens. This can limit the types of materials that can be studied and the information that can be obtained. Furthermore, the high-energy electron beam can damage sensitive specimens. Despite these challenges, TEM remains a vital tool in many fields of science and technology. Its ability to provide detailed information about the structure and composition of materials at the atomic scale makes it an invaluable tool for researchers. In this study, we have used the FEI Tecnai G2 20 TWIN TEM to obtain images. The TEM image of pristine $MoSe_2$, suggests the formation of interconnected wrinkled few layers nanosheets morphology, as shown in **Figure 2.6 (b)**. The TEM analysis of prepared materials has been discussed in upcoming respective chapters.

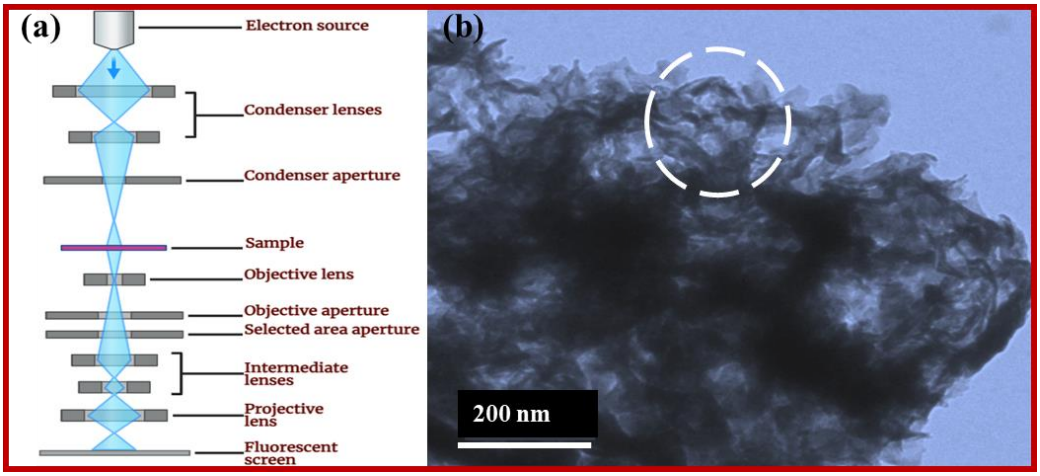

Figure 2.6 (a) *Schematic diagram of TEM and (b) TEM image of pristine* $MoSe_2$.

2.2.4 Raman spectroscopy

Raman spectroscopy is a technique commonly employed for examining the vibrational characteristics of a sample, which is based on the Raman scattering effect of electromagnetic radiation with molecules. The principle of Raman spectroscopy involves the interaction of light with a sample. When a monochromatic light source, such as a laser, incidents on a sample, the light is scattered by the sample's molecules. This scattering can be elastic (Rayleigh scattering), where the scattered light has the same wavelength as the incident light, or inelastic (Raman scattering), where the scattered light has a different wavelength, as shown in **Figure 2.7 (a)**. In Raman scattering, the frequency of the scattered light changes due to the vibrational states, or modes, of a molecule. This change in frequency, known as the Raman shift, is the energy difference between the incident light and the scattered light. The Raman scattering is defined in two ways. The lower frequency shift than the incident light is known as Stokes scattering, and the higher frequency shift than the incident light is known as anti-Stokes scattering. In the present thesis, we have utilized STR-300 micro-Raman spectrometer, equipped with a 532 nm laser source with a power of approximately 1mW at sample. The samples have been examined with a step size of about 1.2 cm^{-1}. The primary components of the Raman spectrometer include the laser, sample chamber, spectrometer and CCD detector. A graphical representation of Raman spectrometer is given in **Figure 2.7 (b)**. As an example, Raman study of pristine $MoSe_2$ is performed to understand its vibrational characteristics, as shown in **Figure 2.7 (c)**. It indicates majorly two vibrational modes E_{1g} and A_{1g}, indicating 2H phase synthesized pristine $MoSe_2$ nanostructure [79-81]. The Raman spectra and their analysis of prepared materials have been discussed in upcoming chapters.

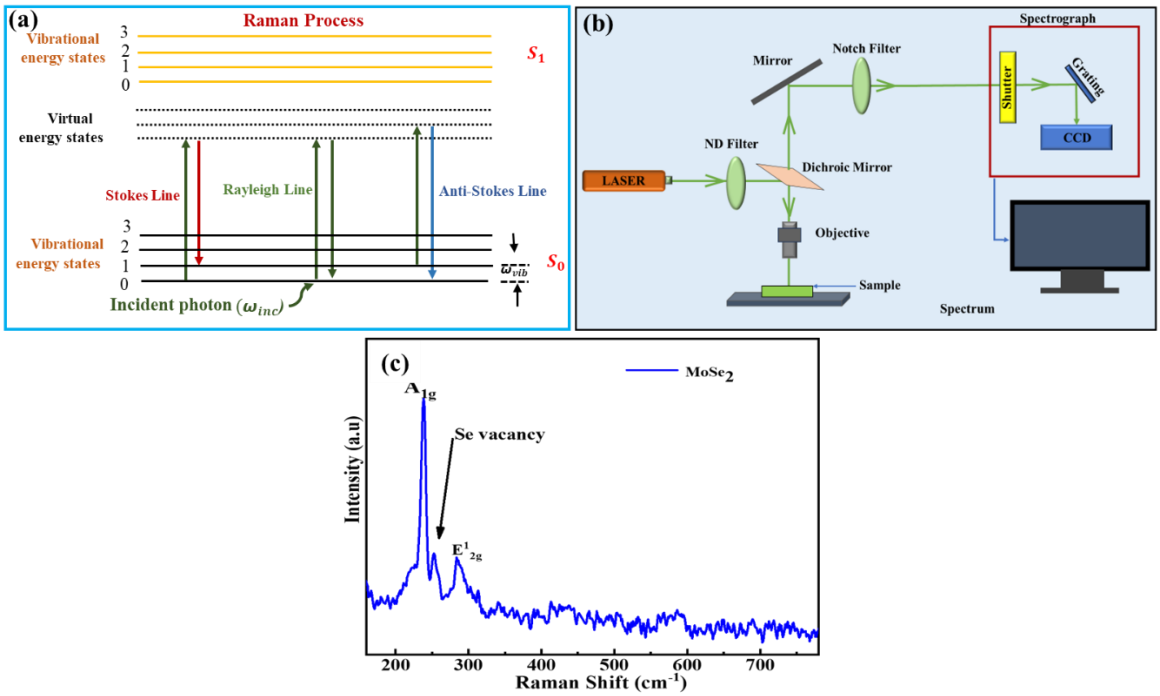

Figure 2.7 *(a) Schematic representation of the various scattering process: Rayleigh, stokes and anti-stokes Raman scattering, (b) graphic representation of Raman spectrometer and (c) Raman spectrum of $MoSe_2$ nanosheets.*

2.2.5 Fourier transform infrared (FTIR) spectroscopy

Fourier Transform Infrared Spectroscopy (FTIR) is a powerful analytical method employed to detect the functional groups present in inorganic and organic materials by measuring their absorption of infrared radiation over a range of wavelengths. FTIR was developed as an improvement over dispersive spectroscopy techniques, which measure intensity over a narrow range of wavelengths at a time. The FTIR spectrum of the synthesized material have been obtained using a ThermoFisher spectrometer. The FTIR spectrometer comprises several components, including a source, beam splitter, interferometer, sample compartment, detector, amplifier, and converter, as illustrated in **Figure 2.8 (a)**. The term "Fourier-transform" in FTIR originates from the fact that a Fourier transform, a mathematical process, is required to convert the raw data into the actual spectrum. The Fourier transform is a mathematical technique that transforms a function of time. The light used in FTIR is infrared radiation, which is absorbed by molecules and causes them to vibrate. One of the key components of an FTIR spectrometer

is the interferometer. The interferometer operates based on the same scientific concepts that are employed in the Michelson–Morley experiment. The interferometer in an FTIR spectrometer is used to generate a beam of light containing many frequencies at once. As an example, FTIR spectrum of $MoSe_2$ nanosheets is given in Figure 2.8 (b), indicating presence of different functional groups. Details of FTIR study for prepared samples have been discussed in upcoming chapters.

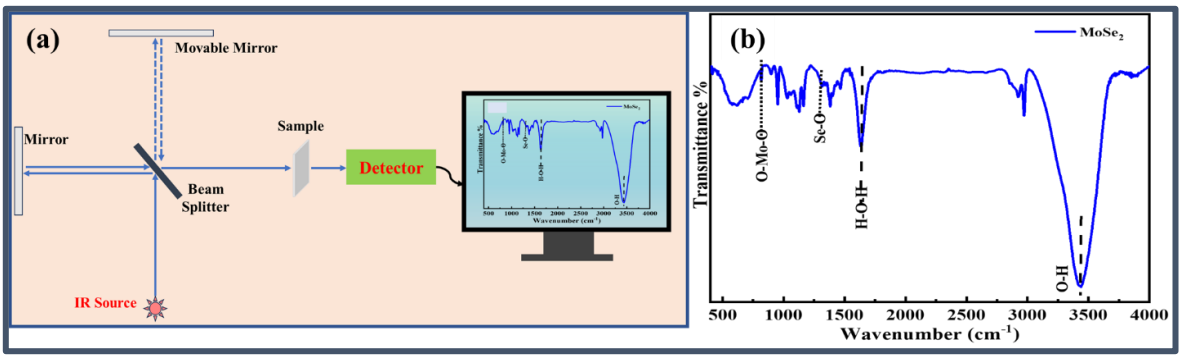

Figure 2.8 *(a) Graphic representation of FTIR spectrometer and (b) FTIR spectrum for pristine $MoSe_2$ nanosheets.*

2.2.6 X-ray photoelectron spectroscopy (XPS)

X-ray photoelectron spectroscopy (XPS) is a quantitative spectroscopic method that is sensitive to the surface of materials. It operates on the principles of the photoelectric effect and is capable of detecting the elements present. XPS can also determine the chemical state and the overall electronic structure and density of the electronic states in the material. The X-rays excite the atoms in the material, causing them to emit electrons, as shown in **Figure 2.9 (a)**. XPS instruments involve irradiating a material with X-ray beam and measuring the kinetic energy of the emitted photoelectrons. The XPS operate in high or ultra-high vacuum conditions to prevent the photoelectrons from being scattered by gas molecules before reaching the detector. X-rays are typically generated by an X-ray tube, and an electron energy analyzer detects the photoelectrons. The resulting spectrum shows the number of photoelectrons/counts versus their binding energy. XPS provides information about the composition and chemical state of the

surface of a material, which is often critical in applications such as catalysis, battery, corrosion, adhesion, and semiconductor device fabrication. As an example, **Figure 2.9 (b)** depicts the survey spectrum of pristine $MoSe_2$, which reveals the existence of characteristic peaks of Mo 3d, Se 3d, and C (carbon peak is due to used carbon paper in measurement). XPS spectra and their analysis of other prepared materials are discussed in upcoming chapters.

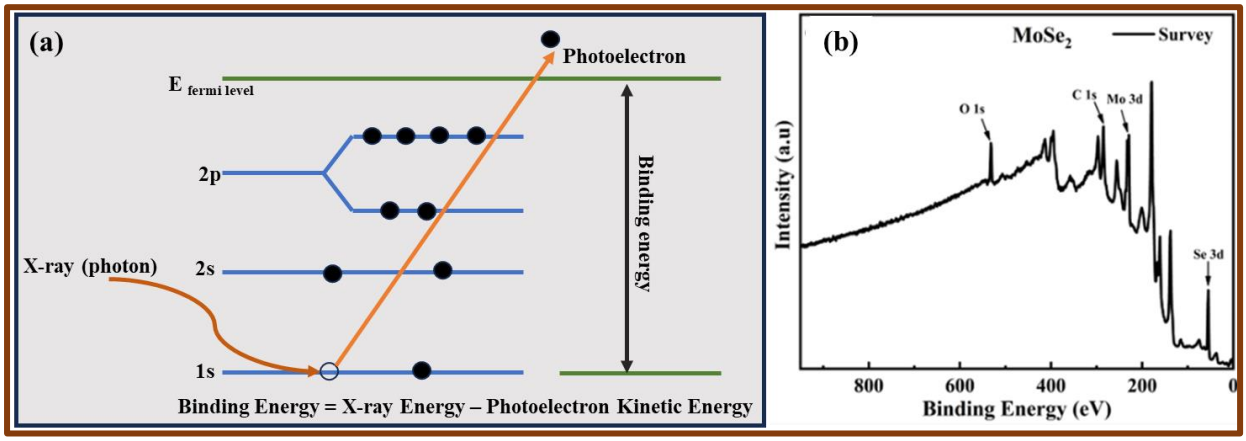

Figure 2.9 *(a) Graphic representation of XPS principle and (b) XPS spectrum for pristine $MoSe_2$ nanosheets.*

2.2.7 Electrochemical techniques

Three-electrode electrochemical system is a fundamental setup in electrochemical experiments, widely used in various fields such as materials science, chemistry, and biology[1]. This system consists of a working electrode, a counter (or auxiliary) electrode, and a reference electrode. A potential is applied between the working and reference electrodes, and the current is measured between working and counter electrode. The current is directly related to the electrochemical reaction rate at the working electrode. Three-electrode system is advantageous because it allows independent control and measurement of the potential and current. This is crucial for studies of electrochemical kinetics and mechanisms. Three-electrode system can be used in a variety of electrochemical techniques, including cyclic voltammetry, chronoamperometry, and impedance spectroscopy. In the present study, all electrochemical

measurements have been measured using CorrTest (CS350) electrochemical workstations. The schematic presentation of three-cell setup for electrochemical studies is given in **Figure 2.10**.

Working electrode

The working electrode is where the reaction of interest occurs. It can be made of solid conducting materials. The nature of the study often determines the choice of the working electrode material. Commonly used solid electrode materials include glassy carbons, conducting carbon paper, carbon cloth, conducting glass, etc.

Counter electrode

The counter electrode, alternatively referred to as the auxiliary electrode, establishes a circuit with the working electrode. This setup guarantees that the reaction under investigation takes place on the working electrode. The counter electrode can participate in a gas evolution reaction or a reaction that is the reverse of the one occurring at the working electrode, thereby maintaining the composition of the electrolyte constant. Platinum is used as a counter electrode for both alkaline and acidic medium.

Reference electrode

The reference electrode serves as a benchmark for gauging and managing the potential of the working electrode, all while not conducting any current. The potential of the working electrode is controlled and measured against the reference electrode.

In this present study, the potential is measured using Hg/HgO (for alkaline medium) and Ag/AgCl (for acidic medium) as reference electrodes. Nernst equation converts recorded potentials to the reversible hydrogen electrode (RHE) potentials [82].

$$E_{RHE} = E_{Hg/HgO} + 0.059 \times pH + 0.098 \quad (5)$$

$$E_{RHE} = E_{Ag/AgCl} + 0.059 \times pH + 0.198 \quad (6)$$

The LSV curves are corrected by manual 90% iR drop correction using the **equation 7** [83].

$$E_{RHE}(iR\ corrected) = E_{RHE} - E_{iR} = E_{RHE} - (I_{measured} \times R_u) \quad (7)$$

where E_{RHE}, $I_{measured}$, and R_u are measured potential, current, and uncompensated resistance, respectively.

The three-electrode system is advantageous because it allows independent control and measurement of the potential and current. This is crucial for studies of electrochemical kinetics and mechanisms. This system can be used in a variety of electrochemical techniques, including cyclic voltammetry, chronoamperometry, and impedance spectroscopy.

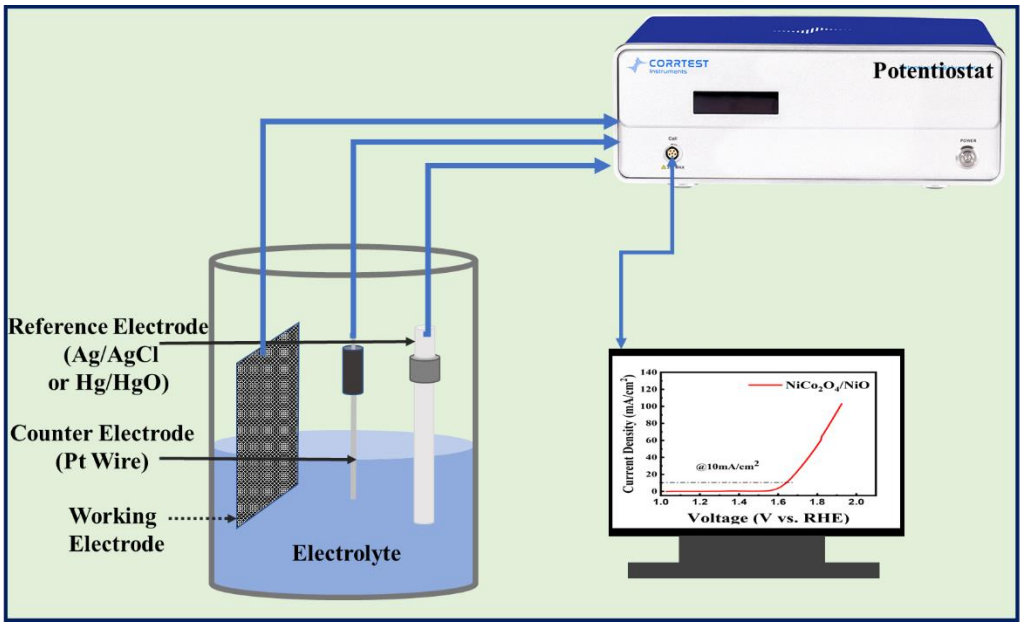

Figure 2.10 *Graphic representation of three cell electrochemical setup.*

2.2.7.1 Linear sweep voltammetry (LSV)

The LSV is utilized for quantitative electrochemical analysis of reaction using reactions using a three-electrode setup. LSV curve is recorded within a specified potential range, from a lower to an upper limit, at a steady voltage sweep rate (v), as shown in **Figure 2.12 (a)**. Electrochemical reactions occur on the working electrode, with the applied potential being linearly swept over time, and the typical current is measured as a function of potential, as illustrated in **Figure 2.12 (b)**. The potential scan typically begins when no electrochemical reaction occurs and is steadily increased at a constant scan rate, ranging from a few millivolts per second (mV s^{-1}) to hundreds of mV s^{-1} until a final potential is attained. The system requires

more time to record the LSV response at a low potential sweep rate. Consequently, the size of diffusion layer will vary depending on the voltage scan rate. In other words, ions have more time to diffuse at slower voltage sweep rates. We have utilized the LSV technique to assess the HER, OER and electrolyzer performance activity.

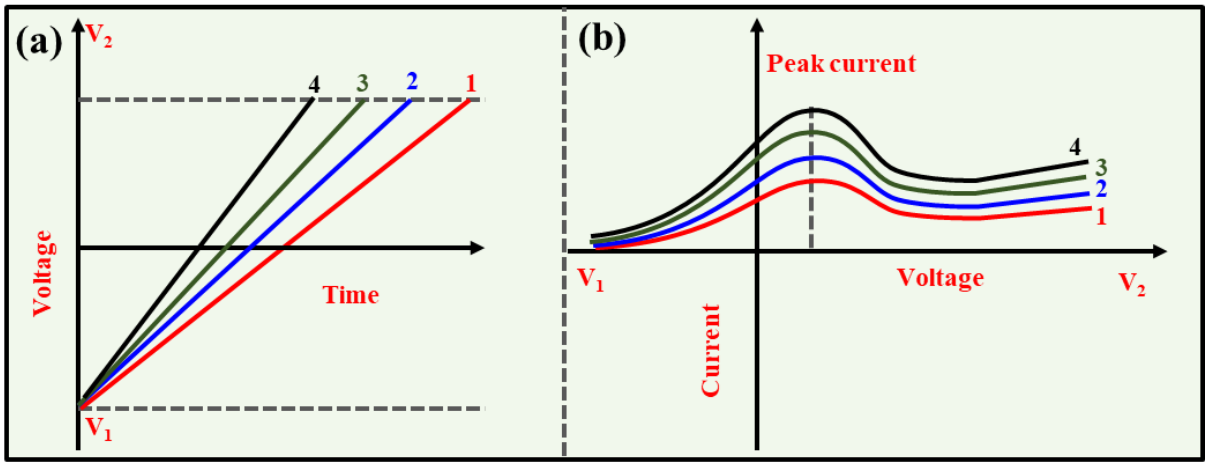

Figure 2.11 *(a) Linear voltage sweep with respect to time and (b) LSV curve at different voltage sweep rates*

2.2.7.2 Cyclic voltammetry (CV)

Cyclic Voltammetry (CV) is a potent electrochemical method that record the current output of a redox-active solution to a linearly cycled potential scan. It is a type of potentiodynamic measurement where the potential of working electrode is ramped linearly versus time in the opposite direction to return to the initial potential after reaching the set potential, as shown in **Figure 2.12**. The current at the working electrode is plotted against the applied voltage to give the cyclic voltammogram trace. It provides quick information about redox processes. The potential scan usually starts at a value where no electrochemical reaction occurs and is increased at a constant scan rate, typically ranging from a few mV s^{-1} to hundreds of mV s^{-1}. We have utilized the CV technique to calculate the electrochemical active surface area (ECSA) of prepared materials by recording CVs at different potential sweep rates within a small potential window of non-faradaic regions.

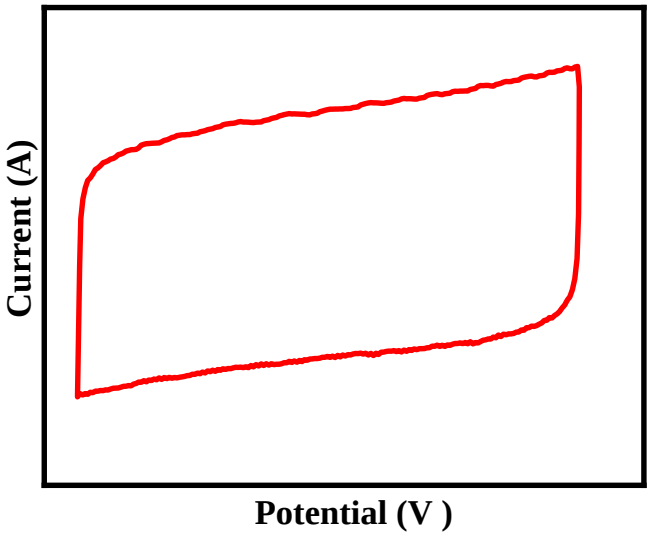

Figure 2.12 *Schematic illustration of typical CV curve.*

2.2.7.3 Electrochemical impedance spectroscopy (EIS)

Electrochemical Impedance Spectroscopy (EIS) is an highly responsive analytical method employed to determine the electrical behavior of chemical systems without causing any damage. The EIS methods is often classified as an AC technique due to the usual sinusoidal stimulation waveform. In EIS study, small amplitude AC potential/current is used in large frequency range to examine the impedance of the electrochemical system. In the present thesis, impedance data is recorded by applying an alternative voltage of low amplitude (5 to 10 mV) across a broad frequency range (0.01 to 106 Hz), at constant DC voltage. The results are graphically represented in the form of Nyquist plots. Nyquist plots are a common graphical representation used in EIS to study electrocatalytic materials. These plots are essentially a way to visualize the impedance of a system as a function of frequency. In a Nyquist plot, the real part of the impedance (Z') is plotted on the x-axis, while the negative of the imaginary part of the impedance (-Z'') is plotted on the y-axis, as shown in Figure 2.13. Each point on the Nyquist plot corresponds to a specific frequency, with high frequencies represented by points near the origin and low frequencies represented by points farther from the origin. The diameter of the semicircle corresponds to the charge transfer resistance (Rct) for the electrochemical reaction.

The point at which the semicircle intersects the x-axis at high frequencies corresponds to the internal resistance (Rs), and the point at which it intersects the x-axis at low frequencies corresponds to the sum of Rs and Rct. A smaller semicircle in the Nyquist plot indicates a lower charge transfer resistance, which suggests that the electrocatalytic material has a higher catalytic activity.

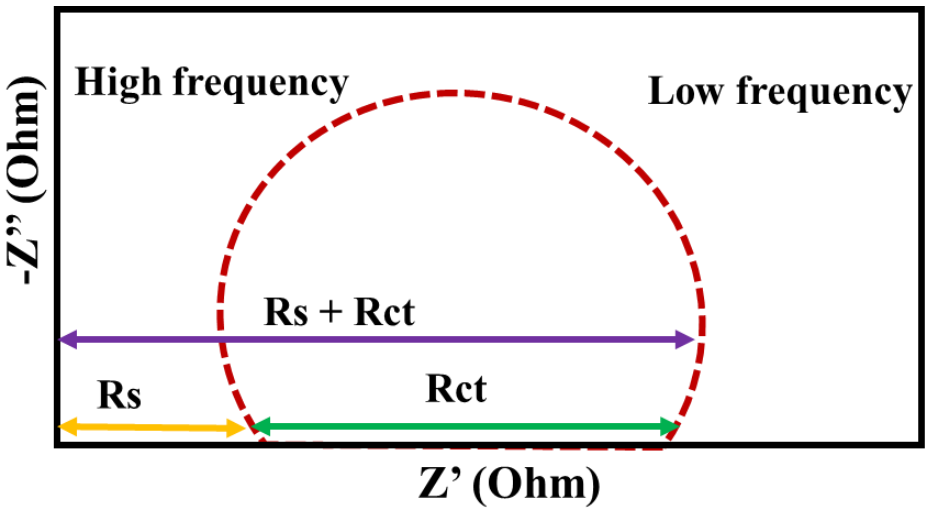

Figure 2.13 *Schematic illustration of typical Nyquist plot for catalytic behavior.*

2.2.7.4 Galvanic charge-discharge measurement

Galvanic charge-discharge measurement is an essential method used in the study of electrochemical energy storage systems. This technique involves applying a constant current to batteries, supercapacitors, or electrode materials to charge and discharge them between defined voltage limits. In GCD process, a constant current is applied until a given potential is reached and the output is plotted as potential vs time, as shown in **Figure 2.14**. This allows researchers to understanding the performance of the battery under different conditions and can help in the design of more efficient and durable batteries. In the present thesis, the rechargeable capability and stability of prepared Zn-air batteries are tested with 5 minutes of charging and discharging cycles, each at the current density of 10 mA cm^{-2}.

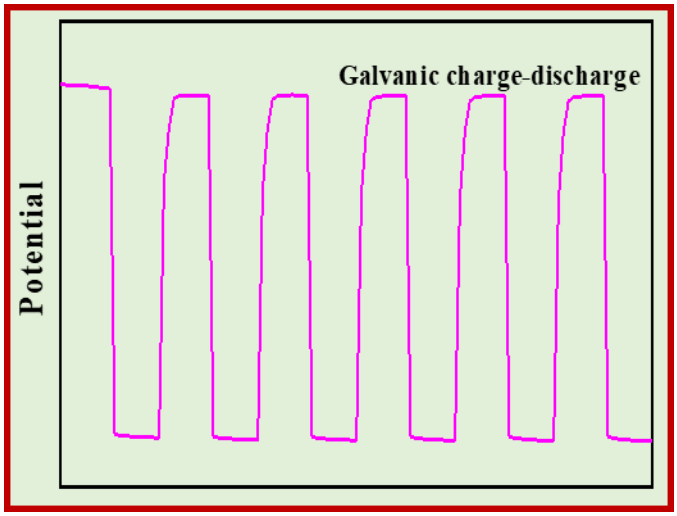

Figure 2.14 *Schematic illustration of Galvanostatic charge-discharge behavior of the battery.*

2.2.8 Experimental details for electrochemical measurements

To prepare electrode, slurry solutions were obtained by dispersing 20 mg of material in 100 µL of IPA. Then, 10 µL of 5% nafion solution (from Sainergy fuel cell India Pvt. Ltd) is added as a binder in the respective slurry solution and sonicated for 5 minutes to achieve uniform dispersion. The homogeneously dispersed solutions are brush-coated over a 1 cm^2 of conducting carbon papers (from Sainergy fuel cell India Pvt. Ltd) to prepare different working electrodes. To reduce the binder effect, the coated electrodes were dried overnight in a vacuum oven at 120 °C. These working electrodes were used for electrochemical studies (HER, OER) of prepared materials in three-cell configuration. The HER studies were performed using LSV at potential sweep rate of 2 mV s^{-1} in an acidic electrolyte (0.5 M H_2SO_4) within a voltage window of 0 to -0.7 V vs Ag/AgCl, while in alkaline electrolyte (1M KOH) within voltage window of -0.924 to -1.424 V vs Hg/HgO. The OER studies are performed using LSV at potential sweep rate of 2 mV s^{-1} in 1M KOH within voltage window of 0 V to 1 V vs Hg/HgO. The EIS study for HER and OER has been done in a frequency range of 0.01 Hz to 10^5 Hz at constant overpotential (-1.23 V vs Hg/HgO for HER and 0.65 V vs Hg/HgO for OER) with AC amplitude of 5 mV. The long-term durability of HER/OER catalyst has been evaluated using chronoamperometry technique at constant applied potential.

2.2.9 Design of aqueous alkaline electrolyzer

An electrochemical overall water splitting device (alkaline electrolyzer) has been fabricated that uses $MoSe_2$ based electrodes. For preparing electrode, slurry solution are prepared by previously discussed in previous section 2.2.8 and coated over two conducting carbon paper of 1 cm x 1 cm. The electrolytic chamber was filled with alkaline electrolyte (1M KOH). Two electrode chambers are separated by PVA-KOH based membrane to avoid gas mixing. To make the PVA-KOH membrane, 2 g of PVA is dissolved in 15 mL of DI water by heating at 90 °C. The KOH solution (2 g of KOH in 5 mL of DI water) is added dropwise to avoid agglomeration with the PVA solution. The final mixture is placed in flat petri-dish and allowed to cool overnight at -23 °C to make a thin film membrane for gas separating membrane in electrolyzer. This indigenously designed electrolyzer fabricated using acrylic sheet (locally available). The electrolyzer has a total cell capacity of 8 mL for the electrolyte (an aqueous 1M KOH solution) and features two interchangeable electrode support structures that serve as supports for the cathode and anode. The power connection terminals for the electrodes are easily accessible from the outside. **Figure 2.15 (b)** shows the image of ingeniously designed electrochemical electrolyzer along with gas collection arrangement via water displacement method.

Figure 2.15 *Photograph of indigenously designed electrolyzer setup showing production of H_2 and O_2.*

2.2.10 Design of zinc-air battery

A Zinc-air cell has been fabricated using prepared materials coated carbon cloth as a cathode and a zinc metal sheet (200 µm thick) as anode for energy storage in the Zn-air battery system. Both electrodes are taken of 1 cm^2 dimensions and fixed on either side of the electrolytic chamber. For preparing the air electrode, the slurry solution is prepared by the same method discussed in previous section 2.2.8 and coated over conducting carbon cloth of 1 cm x 1 cm. The electrolytic chamber is filled with alkaline electrolyte (6M KOH + 0.2 M $Zn(CH_3CO_2)_2.2H_2O$).

Figure 2.16 *Different components and assembled Zinc-air battery.*

Figure 2.16 shows the image of indigenously designed Zinc air battery device fabricated using an acrylic sheet. The battery cell is a prototype with a total cell capacity of 2 mL for electrolyte. It has two replaceable electrode support structures which serve as a support to the cathode and anode. The cell has been equipped with connections to both electrodes. The power connection terminals of electrodes are freely accessible from the outside. The electrode replacement is made exceedingly simple by the design of the device. The OCP, specific capacity, energy density, and power density of designed batteries have been calculated to understand their performance.